APPLIED SCIENCES AND ENGINEERING

Neuronavigation-guided focused ultrasound for transcranial blood-brain barrier opening and immunostimulation in brain tumors

Ko-Ting Chen[1,2], Wen-Yen Chai[3], Ya-Jui Lin[1,4], Chia-Jung Lin[5], Pin-Yuan Chen[6,7], Hong-Chieh Tsai[1], Chiung-Yin Huang[8], John S. Kuo[9], Hao-Li Liu[5]*, Kuo-Chen Wei[1,7,8]*

Focused ultrasound (FUS) in the presence of microbubbles can transiently open the blood-brain barrier (BBB) to increase therapeutic agent penetration at the targeted brain site to benefit recurrent glioblastoma (rGBM) treatment. This study is a dose-escalating pilot trial using a device combining neuronavigation and a manually operated frameless FUS system to treat rGBM patients. The safety and feasibility were established, while a dose-dependent BBB-opening effect was observed, which reverted to baseline within 24 hours after treatment. No immunological response was observed clinically under the applied FUS level in humans; however, selecting a higher level in animals resulted in prolonged immunostimulation, as confirmed preclinically by the recruitment of lymphocytes into the tumor microenvironment (TME) in a rat glioma model. Our findings provide preliminary evidence of FUS-induced immune modulation as an additional therapeutic benefit by converting the immunosuppressive TME into an immunostimulatory TME via a higher but safe FUS dosage.

INTRODUCTION

Glioblastomas (GBMs) are the most common (accounting for 47.7%) malignant primary adult brain tumors, and they carry the worst prognosis with a median overall survival of 14 to 17 months and a 5-year survival of only 5.6% (*1*, *2*). In contrast with recent advancements in GBM diagnostics (such as genome-wide molecular profiling studies), current standard treatment modalities for patients with GBM have unsatisfactory survival improvement (*3*). The infiltrative growth of GBM cells into the adjacent brain has rendered patients with GBM incurable by surgical resection alone, and tumor recurrence is nearly universal (*3*–*5*). Chemoradiation therapy remains the standard of care (SOC) for patients with newly diagnosed GBM after surgery since 2005 (*6*), while no SOC has been established for patients with recurrent GBM (rGBM) (*7*, *8*). Tumor-treating fields (TTFs), using alternating electrical fields to induce mitotic tumor cell death, have been shown to add survival benefit for patients with newly diagnosed but not rGBM (*9*–*11*). The urgent unmet need to improve survival of patients with GBM is reflected by the numerous ongoing trials with many different therapeutic approaches (*3*).

Brain homeostasis is critically regulated by the blood-brain barrier (BBB) (*12*). An integrative BBB is composed of endothelial cells, tight junctions, pericytes, and astrocytes that form neurovascular units, which provide protective and neurophysiological functions for the BBB (*13*, *14*). It has been shown that up to 95% of therapeutic agents are excluded from the brain by the BBB's dual nature as a barrier. As a physical barrier, it allows only hydrophobic and small (<400 Da) molecules to enter via diffusion, and as a chemical barrier, it imports or pumps out proteins or drugs via active transport mechanisms (*14*–*16*). Although the BBB is partially disrupted during GBM progression, the blood-tumor barrier (BTB) can also limit optimal drug accumulation in brain tumors (*12*, *14*, *17*, *18*). Several strategies have been investigated to overcome BBB and BTB and are categorized into physical and nonphysical methods (*19*). By physical methods, BBB tight junctions can be opened using osmotic agents (*20*, *21*), intracranial injection or implantation (*22*, *23*), and convection-enhanced delivery of therapeutic agents (*24*); nonphysical methods such as nonspecific or receptor-mediated uptake are achieved by modifying and targeting therapeutics (*22*).

Focused ultrasound (FUS) combined with intravenous administered microbubbles (MB-FUS) can achieve reproducible, focal, transient, and noninvasive BBB/BTB opening to enhance the targeted permeability of therapeutics (*25*–*28*). In preclinical models of malignant brain tumors, MB-FUS has successfully enhanced the penetration of various drugs (*29*–*32*) and multifunctional agents (*33*–*35*) and was shown to be associated with improved antitumor efficacy (*30*). Nevertheless, the brain tumor microenvironment (TME), especially in GBM, is generally immunosuppressive, causing anergy and exhaustion of antitumor immune cells or converting to protumorigenic activities (*18*, *36*). MB-FUS provides dual effects in immune modulation of TME. First, it was shown to enhance delivery of immunostimulating agents such as interleukin-12 (*37*) and the immune checkpoint inhibitor anti–cytotoxic T-lymphocyte antigen 4 (CTLA-4) antibody (*38*) into tumors. Second, the physical effects produced by MB during FUS treatment were demonstrated to enhance both innate immunity (*39*) and adaptive immunity (*40*).

On the basis of substantial preclinical evidence, clinical trials using MB-FUS with various devices have been initiated since 2014. A total of six trials have been registered targeting patients with GBM with and without chemotherapy using devices including SonoCloud (CarThera Inc.), ExAblate (INSIGHTEC Inc.), and NaviFUS (NaviFUS

[1]Department of Neurosurgery, Chang Gung Memorial Hospital at Linkou, Taoyuan, Taiwan. [2]Ph.D. Program in Biomedical Engineering, Chang Gung University, Taoyuan, Taiwan. [3]Department of Diagnostic Radiology and Intervention, Chang Gung Memorial Hospital at LinKou, Taoyuan, Taiwan. [4]The Graduate Institute of Biomedical Sciences, Chang Gung University, Taoyuan, Taiwan. [5]Department of Electrical Engineering, National Taiwan University, Taipei, Taiwan. [6]Department of Neurosurgery, Chang Gung Memorial Hospital at Keelung, Keelung, Taiwan. [7]School of Medicine, Chang Gung University, Taoyuan, Taiwan. [8]Department of Neurosurgery, New Taipei Municipal TuCheng Hospital, Chang Gung Medical Foundation, New Taipei, Taiwan. [9]Department of Neurosurgery and Mulva Clinic for the Neurosciences, Dell Medical School, The University of Texas at Austin, Austin, TX 78712, USA.
*Corresponding author. Email: kuochenwei@cgmh.org.tw (K.-C.W.); hlliu@ntu.edu.tw (H.-L.L.)

Inc.) (*19*). In contrast to SonoCloud, which requires open surgical implantation, and ExAblate, which requires performing the entire procedure in a magnetic resonance imaging (MRI) suite using stereotactic frame fixation on the patient's head, NaviFUS uses a clinically available neuronavigation system to guide the FUS procedure (*41*). Through personalized simulation of focal beam and skull attenuation in combination with the neuronavigation system, NaviFUS intraoperatively steers the transcranial burst-mode ultrasound energy precisely toward targeted central nervous system (CNS) regions.

Here, a rat xenograft model of human malignant glioma helps elucidate the potential immune response of TME at different time points after MB-FUS treatment; it serves as an equivalent experiment design to complement the human clinical trial study by compensating for limitations that prevented TME study in human participants. We report comprehensive parallel results between human patients and the rat model with regard to the phase 1 pilot study for the evaluation of safety, feasibility, and tolerated dose of BBB opening for NaviFUS MB-FUS treatment. Evaluation of BBB permeability by dynamic contrast-enhanced MRI (DCE-MRI) and the composition of immune cells in the TME from surgically resected tissues in both clinical and preclinical studies are also reported. In this study, the preclinical testing helped reveal a more in-depth and insightful understanding of the accompanying immunoregulatory effect by investigating a wider ultrasound exposure range and longitudinal histological examinations that can potentially circumvent clinical challenges.

RESULTS

Clinical findings

Participants

Table 1 summarized patient demographics in this study. Six patients were enrolled, three men and three women, with a mean age of 49.5 years (range, 32 to 80 years old). The mean body weight was 69.4 kg, and mean body mass index was 25.0 kg/m^2. The sites of sonication were all at peritumoral regions adjacent to enhancing tumor or fluid-attenuated inversion recovery (FLAIR) hypersignal area if no enhancing tumor was detected on preoperative MRI. The mean depth from the inner skull to the sonicated targets was 3.85 cm (range, 3.1 to 4.7 cm). Locations of sonication were subcortical or periventricular, with four frontal lobes, one temporoinsular, and one occipital lobe. Only two severe adverse events (SAEs), which were unrelated to FUS treatment, hyponatremia and hypernatremia, occurred in patient 1, who received exposure level not exceeding 0.48 mechanical index (MI).

Table 2 summarized the detailed parameters of the different estimated ultrasound exposure ceiling levels, including 0.48 (0.43 ± 0.05), 0.58 (0.53 ± 0.05), and 0.68 (0.63 ± 0.05) MI, respectively. A range rather than a specific energy level was reported because of the consideration that ~10% of uncertainty exists between the planned exposure level for personalized treatment l and the actual deposited one. The intravenous administration of MB was 4.8 ml. Although each treatment had its own starting location and path, the planned trajectories in this study all started from the frontal bone or parietal bone with a mean skull thickness of 7.25 and 10.25 mm, respectively. The overall mean computed tomography (CT) number was 1396.1 ± 65.3 Hounsfield units. The mean estimated transcranial efficiencies were 30.06, 26.0, and 24.26%, respectively, at the three levels of FUS energy. A mean time of 95 min (range, 78 to 135 min; from preoperative to postoperative preparation) was needed for the entire procedure. Among these, the mean operation time was estimated to be 14.2 min (ranging from 5 to 22 min; including neuronavigation registration time and FUS sonication time range).

Primary outcome

The primary end point for this study was safety of BBB opening after NaviFUS treatment. A total of 36 adverse events (AEs) happened in five patients (five of six; 83%) during the post-FUS

Table 1. Summary of patients with rGBM receiving FUS treatment: demographic data and treatment plans (*n* = 6). BW, body weight; BMI, body mass index; Preop, preoperative; M, male; F, female; KPS, Karnofsky performance status.

Patient number	1	2	3	4	5	6	Means ± SD
Level	1	1	2	2	3	3	
Age	80	39	32	36	67	43	49.5 ± 19.4
Sex	M	F	M	M	F	F	
BW (kg)	63	55	82.5	2.1	69	54.5	69.4 ± 15.2
BMI (kg/m^2)	22.6	21.6	25.5	29.8	27	23.6	25.0 ± 3.1
Preop KPS	70	100	100	100	70	100	
Definition of progressive disease*	New enhancing lesion	Increase in FLAIR	New enhancing lesion	Increase in FLAIR	New enhancing lesion	New enhancing lesion	
Site of sonication	Peritumoral	Peritumoral	Peritumoral	Peritumoral	Peritumoral	Peritumoral	
Location	Temporoinsular	Frontal periventricle	Frontal subcortical	Frontal periventricle	Frontal subcortical	Occipital periventricle	
Depth from inner skull (cm)	4.1	3.9	3.1	4.6	2.7	4.7	3.85 ± 0.80
SAE (times)	2†	0	0	0	0	0	

*Progression of tumor was defined according to response assessment in neuro-oncology for gliomas (RANO) criteria, including new enhancing lesion or notable increase T2/FLAIR nonenhancing region. †All SAEs occurred in this study were judged as definitely not related to the FUS treatment and SonoVue in causality.

Table 2. Summary of cranial bone, exposure conditions, and degree of BBB permeability via DCE-MRI evaluation ($n = 6$). HU, Hounsfield units.

Patient number	1	2	3	4	5	6
Exposure level	1	1	2	2	3	3
Estimated ceiling MI†	0.48 (0.43 ± 0.05)	0.48 (0.43 ± 0.05)	0.58 (0.53 ± 0.05)	0.58 (0.53 ± 0.05)	0.68 (0.63 ± 0.05)	0.68 (0.63 ± 0.05)
SonoVue dose (ml)	4.8	4.8	4.8	4.8	4.8	4.8
Location of penetration	Parietal bone	Frontal bone	Frontal bone	Frontal bone	Frontal bone	Parietal bone
Estimated skull thickness (mm)	8.5	8	6	6	9	12
Mean CT number of skull (HU)	1326.29	1422.95	1513.71	1370.9	1366.76	1376
Estimated transcranial efficiency (%)	37.18%	22.94%	27.91%	24.1%	23%	25.51%
Overall procedure time (min)*	135	129	78	115	82	78
Operation time (min)†	21	22	11	5	8	18
MRI CE-T1 increase (%)/*P* value	1.736 ± 3.458% /0.1705	1.514 ± 2.036% /0.0561	1.738 ± 2.200% /0.0452	3.797 ± 4.859% /0.0471	8.323 ± 10.24% /0.0406	2.979 ± 1.775% /0.0010
K_{trans} increase (min^{-1})	0.0061 ± 0.004	0.0045 ± 0.003	0.0107 ± 0.012	0.0173 ± 0.014	0.0202 ± 0.007	0.0113 ± 0.003
V_e increase	0.0059 ± 0.004	0.0049 ± 0.003	0.0131 ± 0.002	0.0204 ± 0.013	0.0272 ± 0.015	0.0193 ± 0.0129

*Overall duration including the preoperative and postoperative preparation time. †Navigation setup and FUS treatment duration.

1-month follow-up period (see tables S1 to S4). Two SAEs were noted in this study, which were hyponatremia and hypernatremia, and these all occurred in patient 1 (80 years old), who received level 1 energy dose (0.48 MI). No AEs were determined to be related to FUS treatment or MB. There were no deaths, hemorrhages, brain swelling, or neurologic deficits on the day of procedure or during follow-up. There was no dose-limiting toxicity (DLT) and no AEs that aborted the procedures. Radiologically, there was no evidence of intracerebral hemorrhage or swelling (fig. S1). Therefore, NaviFUS treatment was determined safe and tolerable for all patients in this study.

Secondary outcome

Figure 1 shows an example of BBB permeability immediately and 24 hours after NaviFUS treatment, represented by contrast-enhanced T1 MRI (CE-T1) and K_{trans} maps from a low-dose exposure patient (patient 2; exposure level 1; estimated ceiling level of 0.48 MI). Under the lower exposure level, the signal intensity change (SIC) was not statistically significant when comparing the time points of immediate (0.5 hours) and 24 hours after FUS exposure from CE-T1 maps (from 2.52 ± 0.78% to 0.41 ± 1.18%, $P > 0.05$); however, the SIC was statistically significant when comparing the time points in the K_{trans} map (from 0.0069 ± 0.0018 min^{-1} to 0.0012 ± 0.001 min^{-1} in K_{trans}, $P < 0.05$), providing evidence that the BBB at the target regions had been opened.

For comparison, Fig. 2 presents another example showing the CE-T1 and K_{trans} maps obtained from a high-dose exposure patient (patient 6; exposure level 3; estimated ceiling level of 0.68 MI). At this level, both CE-T1 and K_{trans} maps showed statistically significant SIC when comparing the time points at immediate (0.5 hours) and 24 hours after FUS exposure (from 9.32 ± 12.47% to 5.25 ± 1.67% in CE-T1, $P < 0.005$; and from 0.0113 ± 0.0031 to 0.0018 ± 0.0011 min^{-1} in K_{trans}, $P < 0.005$). This demonstrated that elevated FUS energy delivery induced increased size of BBB opening at the FUS targeted position. Images obtained from all six patients were listed in fig. S2.

BBB successfully and transiently opened at target region

The summary of SIC of CE-T1 and DCE-T1 MRI (K_{trans} and V_e) immediately and 24 hours after FUS exposure for all patients is shown in Table 2 and Fig. 3. Since all participants were included on the basis of their diagnostic MRI, typically only CE-T1 was presented. Once the patient had been recruited, the participant received a DCE-MRI at day 0 (immediately after FUS) and day 1 (24 hours after FUS). We therefore lack a pretreatment DCE-MRI for a baseline K_{trans} and V_e. Instead, a selection of another tumor peripheral (nonenhanced) region was used as an internal control (Fig. 3). In patients with notable BBB opening, all showed permeability return to near baseline [as demonstrated by similar signal intensity (SI) to the peripheral control area], which provided information regarding the normalization of BBB permeability in a 24-hour period (Fig. 3 and fig. S2). In level 1 (0.48 MI as the estimated ceiling level) group, no statistically significant SIC was observed in CE-T1 MRI series, but the K_{trans} increment was statistically significant (300.46% in K_{trans} change with $P = 0.0165$ and 302.75% in V_e change with $P = 0.0287$; Fig. 3). In higher-level (0.58 and 0.68 MI as the estimated ceiling level, respectively) groups, the SIC analyses were all significantly enhanced (323.63 and 653.02% in K_{trans} change with $P = 0.0426$ and $P = 0.0457$ and 354.15 and 1560.71% in V_e change with $P = 0.0355$ and $P = 0.0155$, respectively; Fig. 3). Furthermore, a positive correlation

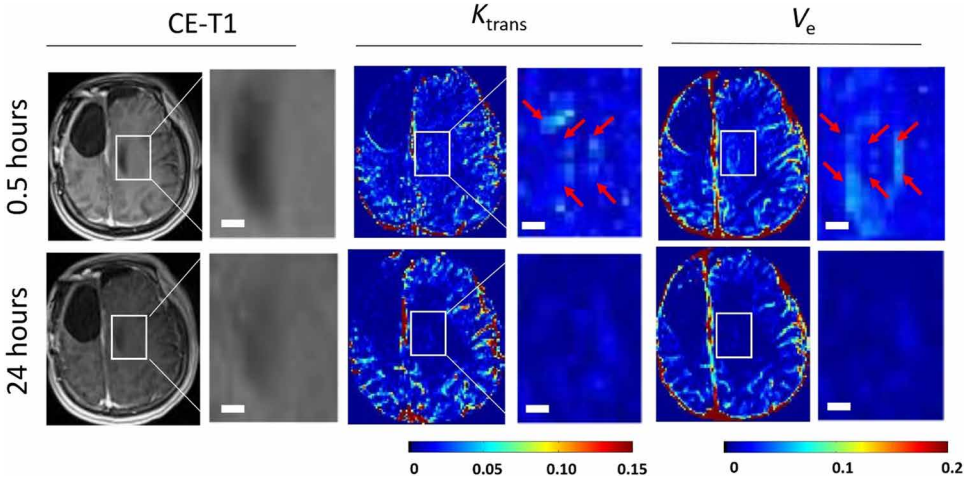

Fig. 1. Evaluation of BBB permeability immediately and 24 hours after FUS treatment in patient 2 (exposure level 1). A 3 × 3 phased array FUS-induced BBB opening (red arrows) is shown in K_{trans} and V_e maps, but not CE-T1 map immediately after treatment (top column). Twenty-four hours later, the BBB permeability returned to baseline as demonstrated by K_{trans} and V_e maps (bottom column). Scale bars, 5 mm.

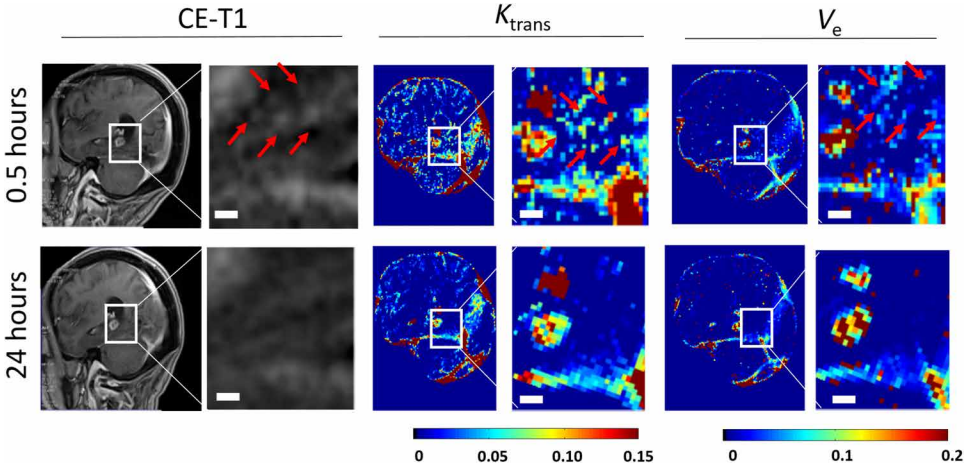

Fig. 2. Evaluation of BBB permeability immediately and 24 hours after FUS treatment in patient 6 (exposure level 3). A stronger 3 × 3 phased array FUS-induced BBB opening (red arrows) is shown in CE-T1, K_{trans}, and V_e maps immediately after treatment (top column). Again, upon posttherapeutic 24 hours, the BBB permeability returned to baseline as demonstrated by K_{trans} and V_e maps, as well as no enhanced dots on CE-T1 imaging (bottom column). Scale bars, 5 mm.

between energy level and SIC was also noted, indicating that higher BBB permeability can be induced with a higher energy of FUS treatment (Fig. 3 and fig. S3).

To summarize, we present the analysis of the non-FUS spot (control area) as proof that only FUS treatment regions exhibited transient MRI SIC. Owing to (i) the permeability of the selected treatment target that is similar to control area and (ii) the control area that did not show any SIC 0.5 and 24 hours after FUS treatment via DCE-MRI, the results support the fact that the FUS transiently regulated BBB permeability and the BBB integrity was returned to baseline, although lack of DCE-MRI at screening phase.

No immunological response 7 days after FUS treatment

There was no notable change observed in the numbers of $CD4^+$, $CD8^+$, $FOXP3^+$ lymphocytes, or $CD68^+$ macrophages in resected samples obtained 7 days after NaviFUS treatment in all participants (Fig. 4). There were sparse lymphocytes infiltrated in adjacent normal brain, peritumoral, or tumor tissues. The major immune-related cell type observed in normal, peritumoral, and tumor tissues was macrophages, but there were no statistically significant differences between the FUS-treated and FUS-untreated samples.

Preclinical findings

Because of limitations in the human study (e.g., restricted parameter range and limited tissue sampling time of 7 days after NaviFUS), we could not fully observe and investigate a previously reported local biological and immunological effect associated with FUS-BBB opening (*19*). We therefore designed a preclinical animal study using a similar parameter (0.63 MI, to mimic exposure level 3 in human trial) and an excessive parameter (0.81 MI to extend the exposure energy) to evaluate whether FUS-BBB opening triggered any local biological and immunological response.

Preclinical evidence of BBB opening

In the rat glioma model, we demonstrated kinetic changes in BBB permeability by DCE-MRI immediately after FUS treatment (Fig. 5).

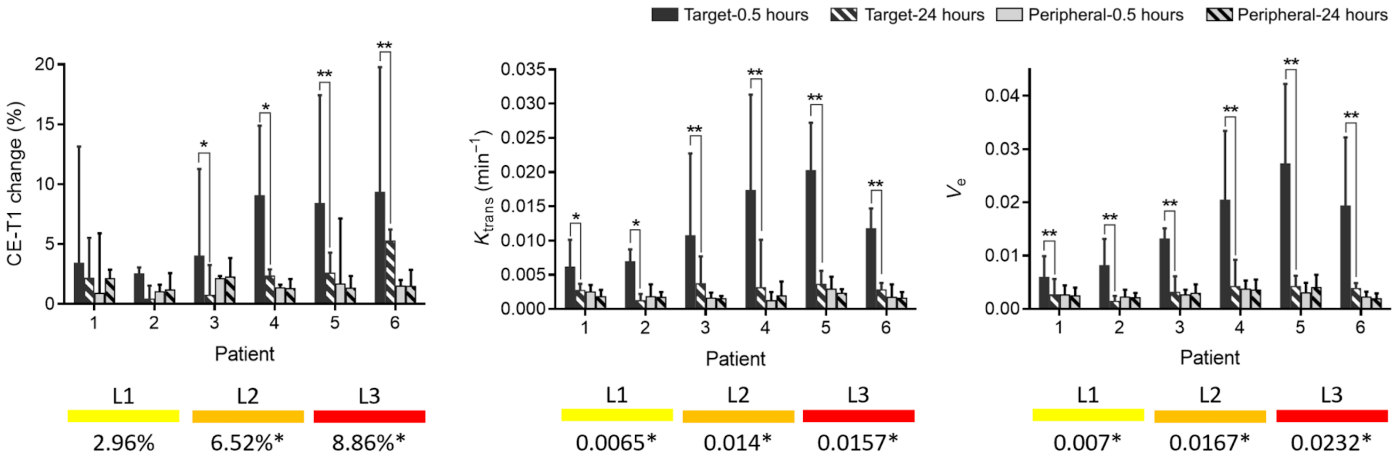

Fig. 3. Statistical analysis of BBB-opened scale evaluated by gadolinium extravasation SIC (**left**) and kinetic parameters including K_{trans} (**middle**) and V_e (**right**) at the time point immediately (0.5 hour) after FUS treatment and 24 hours after treatment. A statistically significant increase in BBB permeability immediately (black slash) after FUS treatment was noted comparing to 24 hours (black bar) after treatment. As an internal control, a non-FUS targeted but same character of tumor peripheral region was selected and measured immediately (gray bar) and 24 hours (gray slash) after treatment, which no SIC change was observed. In sum, a successful BBB opening and subsequent permeability normalization can be observed in all cases. L1, exposure level 1; L2, exposure level 2; L3, exposure level 3. *P < 0.05 and **P < 0.005.

Because of the small size of the rat brain, the FUS-treated area covered both tumoral and peripheral regions simultaneously. Both 0.63 and 0.81 MI (estimated derated level in brain tissue) induced increased gadolinium penetration and increased K_{trans} and V_e maps, suggesting an overall increase in BBB permeability in previously nonpermeable peritumoral regions (Fig. 5, A and B). Furthermore, analysis of SIC comparing tumor, peritumor, and contralateral normal brain before and immediately after FUS treatment showed significant increments of K_{trans} and V_e in peritumoral region using 0.63 and 0.81 MI, respectively (all P < 0.05; Fig. 5, C and D). For peripheral regions, a dose-dependent association was observed when comparing 0.81- to 0.63-MI group [562.81% in K_{trans} change with P = 0.0024 (Fig. 5C) and 770.56% in V_e change with P = 0.0011 (Fig. 5D) in 0.81-MI group], which was also observed in the human study. For tumoral regions, only 0.81 MI further enhanced BBB permeability in K_{trans} and V_e maps [45.69% in K_{trans} change with P = 0.0177 (Fig. 5C) and 54.86% in V_e change with P = 0.0061 (Fig. 5D)], suggesting further opening of an already impaired BBB with higher exposure level. In addition, similar observations of a similar increment of K_{trans} and V_e using the highest exposure level in human study [estimated ceiling level of 0.68 MI (i.e., 0.63 ± 0.05 MI); Fig. 3] and in animals receiving 0.63-MI energy (Fig. 5, C and D) imply an extrapolatable model for further study on the human scale.

Preclinical evidence of immunogenic response of BBB opening

We further analyzed immunological changes at the different time points of days 0 and 7 after FUS treatment under the two given sonication levels. An analytical plot from immunohistochemistry (IHC) staining (fig. S4) is presented in Fig. 6. In the rat model, there was a significant increase in $CD4^+$ lymphocytes 7 days after 0.81-MI FUS treatment in comparison to day 0 (P = 0.043; Fig. 6A). A similar trend showing increased $CD8^+$ lymphocytes was also observed after 0.81-MI exposure (P = 0.056; Fig. 6B). No significant change of $CD68^+$ macrophage or $FOXP3^+$ lymphocyte counts were found (P = 0.17 and P = 0.072, respectively; Fig. 6, C and D). For 0.63-MI exposure, there was no statistically significant increase in $CD4^+$, $CD8^+$ lymphocytes, $CD68^+$ macrophages, and $FOXP3^+$ lymphocytes 7 days after 0.63-MI FUS treatment (P = 0.243, P = 0.176, P = 0.473, and P = 0.525, respectively; Fig. 6, A to D). The above findings suggest that—mimicking NaviFUS treatment of human rGBM patients—no immunogenic response was observed on day 7 after treatment with 0.63-MI FUS in the rat glioma model. However, analysis at day 7 for 0.81-MI FUS treatment showed a significant immunogenic response—particularly for $CD4^+$ [i.e., helper tumor-infiltrating lymphocytes (TILs)] and, to a lesser degree, $CD8^+$ (i.e., cytotoxic TILs). Some animals showed $CD68^+$ macrophage level change but without significant statistical difference, and $FOXP3^+$ lymphocytes were not affected by FUS exposure.

To infer a potential immune modulatory effect using MB-FUS in human, we should carefully assess these following findings: (i) a statistically identical enhancement of BBB opening permeability produced by 0.63-MI FUS exposure in rat glioma model and by 0.63 ± 0.05–MI FUS exposure level in patients with rGBM (Figs. 3 and 5); (ii) no significant immunogenic response observed at day 7 for 0.63-MI exposure in rat glioma model or 0.63 ± 0.05 MI in patients with rGBM (Figs. 4 and 6); and (iii) a significant immunogenic response at day 7 after 0.81-MI exposure in rat glioma model (Fig. 6). On the basis of these findings and the results observed from the parallel animal-human experimental design, it suggests that higher FUS exposure level (0.81 MI) has the potential to trigger TIL-related immune response in human.

DISCUSSION

We demonstrate a safe, reversible, and neuronavigation-guided, noninvasive BBB opening using NaviFUS in patients with rGBM. The tolerated BBB opening dose for NaviFUS system is less than 0.68 MI without any procedure-related AEs or radiological sequela. The device is mobile and integrates with a standard neuronavigation system. It does not require a large space and expensive intraoperative MRI suite, and the procedure is efficient and can easily be performed within 15 min. NaviFUS does not require rigid skull fixation and can achieve target accuracy within an error of deviation of

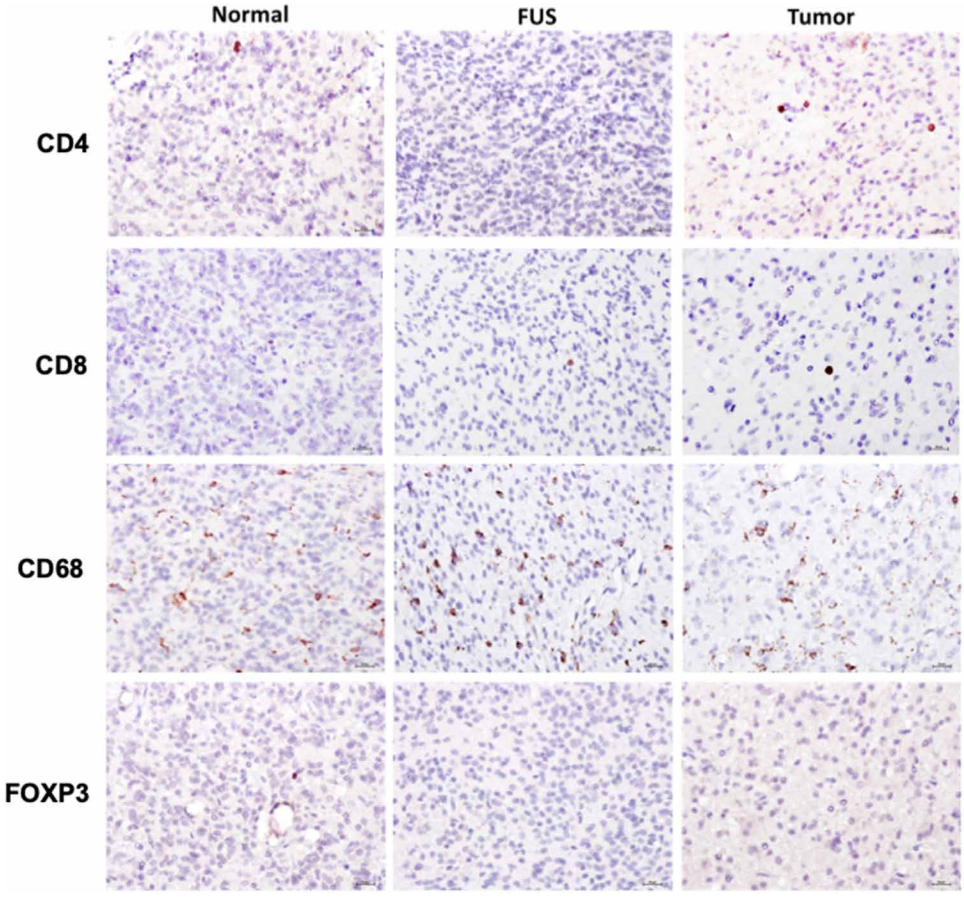

Fig. 4. Immune cell infiltration in human tissues 7 days after FUS treatment. No substantial differences could be identified among peritumoral normal tissues, FUS-treated tissues, and tumor tissues, indicating no immunogenic response 7 days after single-session FUS treatment in human brain. Immune cells of different categories were stained in brown.

less than 3 mm (*41*). In addition, a preclinical model study in parallel revealed an immunomodulatory response at a higher FUS level of 0.81 MI, but not at the 0.63 MI that is similar to the highest tested human trial dose. This dose-dependent effect on BBB opening suggests a possible immunostimulatory effect within the TME with higher energy dose. The above findings suggest that higher-dose FUS may cause potential immunostimulatory effect that might turn an immune "cold" tumor into a "hot" tumor and further support NaviFUS in advancing to next-stage therapeutic trials.

The major obstacles limiting therapeutic efficacy in patients with GBM and rGBM are the BBB/BTB, which prevent drugs from entering into the brain, and a profoundly immunosuppressive TME (*3*, *18*, *36*). MB-FUS has been proven to enhance CNS drug delivery by opening the BBB in animal models (*26*–*28*) and to enhance both innate and adaptive immunities (*39*, *40*). We showed that higher FUS energy at 0.81 MI appeared to induce an immunogenic TME at day 7 in the animal model. Two gaps need to be filled regarding an extrapolation of this finding to human scale. First, a comparative dose intensity relationship should be established between animal model and human scale, which has been demonstrated previously by an identical degree of BBB opening in both species. In addition, the parameters used in preclinical study (except for the exposure level) should be identical to the ones used in clinical trials. For humans: burst length/spot, 10 ms; exposure time/spot, 120 s; in total, $3 \times 3 = 9$ spots; prolactin-releasing factor (PRF)/spot, 1 Hz (or equivalent to PRF, 9 Hz). For animal: burst length, 10 ms; exposure time, 120 s; only single spot; PRF, 1 Hz. Since, in human exposure, the spacing between each adjacent spot is 5 mm, the biological effect in each focus is considered to be isolated and independent (the evidence of sufficient BBB-opened spacing can be supported from the observation of Figs. 1 and 2). Second, there remain doubts as to whether 0.81-MI level is safe to use in humans. Previously, two animal studies have shown that 0.8-MI (*42*) or 0.85-MI (*43*) exposure induced asymptomatic red blood cell (RBC) extravasation and cellular apoptosis after single and multiple FUS treatments, respectively, and no short-term or long-term AEs had been posted. It has also been reported that up to 1.1-MI FUS exposure in human trials did not cause ultrasound dose–related toxicity (*44*). While currently only speculative, it is postulated that these results show the potential of direct immune modulation of TME by MB-FUS in patients with malignant glioma, particularly at the exposure level beyond the one tested in this clinical trial (*44*).

Extensive research aimed at improving GBM/rGBM patient survival is continuously developing. TTF is one successful example for its use of locally applied alternating electrical field to disrupt mitosis of tumor cells, which prolongs both progression free survival (PFS) and overall survival (OS) although a small effect magnitude (*3*, *10*, *11*). Although overall survival is not prolonged, bevacizumab, an anti–vascular endothelial growth factor antibody, is the only available

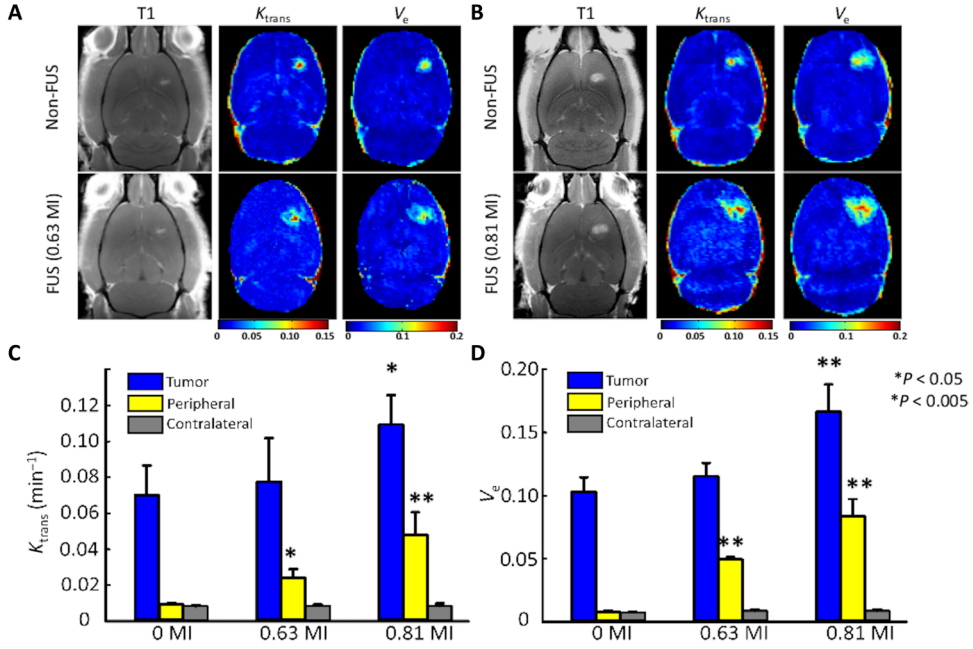

Fig. 5. Kinetic maps derived from DCE-MRI immediately after MB-FUS treatment in rat glioma model. (**A**, **B**) An increased contrast extravasation on T1-weighted imaging, an enhancement of influx volume constant transfer from intravascular to extravascular space (EVS) on K_{trans} map, and an elevation of EVS volume fraction on V_e map are noted. (**C**, **D**) A significant enhancement of K_{trans} and V_e in peritumoral region is demonstrated after 0.63- and 0.81-MI FUS treatment, respectively. Furthermore, a significant increment of the already permeable BBB in tumor region is noted after 0.81 MI.

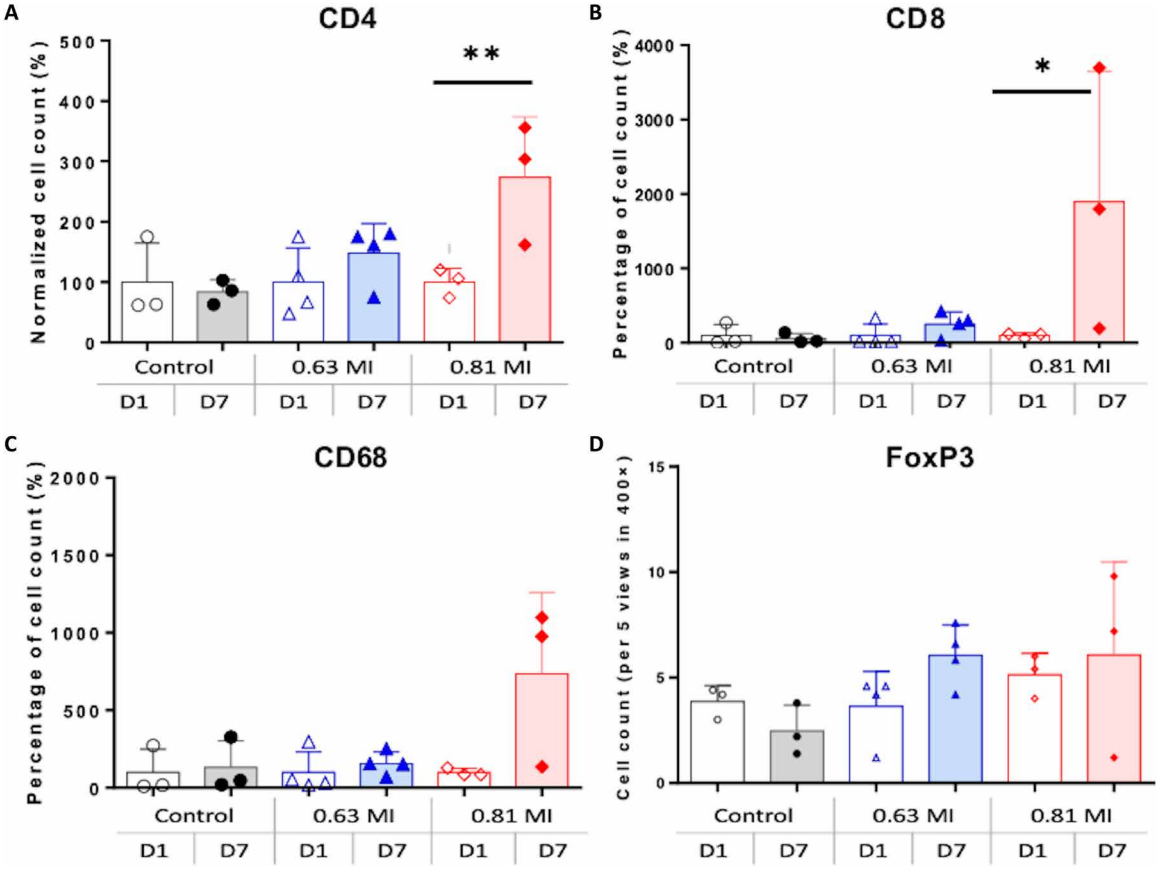

Fig. 6. Immune cells infiltration in tumor tissue immediately and 7 days after FUS treatment in rat glioma model. An increment of $CD4^+$, $CD8^+$ [$P = 0.043$ (**) and $P = 0.056$ (*), respectively, in (**A**) and (**B**)], but not $CD68^+$ macrophages, $FOXP3^+$ lymphocytes [$P = 0.17$ and $P = 0.072$, respectively, in (**C**) and (**D**)], 7 days after 0.81-MI FUS treatment comparing to day 0.

Fig. 7. Schematic diagram of neuronavigation-guided FUS treatment. (**A**) The system is constructed by a FUS phased array system in conjunction with neuronavigation system to intraoperatively guide FUS energy deposition in targeted brain regions. A patient is fixed semirigidly without headpin system. (**B** and **C**) The phased array probe is connected to the power generator and working station by a mechanical arm, which can be adjusted by a physician to match the trajectory and target according to the guidance of neuronavigation. The whole procedure takes less than 1 hour. Photo credits: Ko-Ting Chen, Chang Gung Memorial Hospital at Linkou, Taoyuan, Taiwan.

drug for patients with rGBM who have failed temozolomide chemoradiotherapy (*3*, *7*–*9*). Many therapeutics targeting specific pathways relating to gliomagenesis or restoring immunogenic TME are still being investigated (*3*, *4*, *7*). In addition, multimodality therapeutic strategies have been proposed involving enhanced local drug delivery. Emerging clinical trials using MB-FUS technology combined with therapies for GBM are also in progress (*19*), with initial clinical reports not posting any major hazards and showing preliminary therapeutic benefits (*45*). Using MB-FUS to open the BBB as a complementary treatment could unlock many potential therapies for rGBM.

Two FUS devices have been studied in various brain disorders—including brain tumors—in humans (*19*). Mainprize *et al.* (*46*) have reported the feasibility of using MR-guided FUS (MRgFUS) to deliver chemotherapy in the peritumoral region in patients with newly diagnosed high grade glioma. Carpentier and co-workers (*44*, *45*) used a skull-implanted pulsed ultrasound device, SonoCloud-1, to repeatedly open the BBB concomitant with intravenous carboplatin delivery and showed a positive trend in overall survival for patients with rGBM with clear BBB disruption in comparison to those with minimal BBB disruption. NaviFUS is a new device with several innovative features: (i) It is a mobile all-in-one console that is not limited to the operation room and has a short procedure time (mean time, <15 min per treatment); (ii) its incorporation with neuronavigation system maintains accuracy (mean error, <3 mm) with semirigid fixation of skull (no head pin); and (iii) its manual controllability by physician enables direct monitoring of awake or lightly sedated patients (Fig. 7).

One consideration for incorporating FUS devices into current SOC in patients with GBM/rGBM is the simplicity and cost effectiveness of integration into a clinical setting. In that regard, NaviFUS has shown great potential for further therapeutic strategy in combination with chemotherapies that have been established in several clinical trials using different devices, including carboplatin (*44*) and temozolomide (*47*), in single or repeated treatments (*47*). Moreover, we demonstrated an immunostimulatory potential with FUS alone, which may add another mechanism to overcoming immunosuppressive TMEs, in addition to enhancing monoclonal antibody concentrations. For example, bevacizumab, being reported to pose antitumor immunity (*48*) and has successfully proven its synergy in conjunction with FUS-BBB opening (*49*) but has not been clinically evaluated, may be a suitable candidate in the future.

Another consideration is that the heterogeneity of gray and white matter, distribution of vasculature, and thickness and unevenness of skulls are main considerations when designing FUS devices for translational applications (*19*). While SonoCloud avoids the above issues using an invasive implanted cranial burr hole window design, both MRgFUS and NaviFUS face these engineering

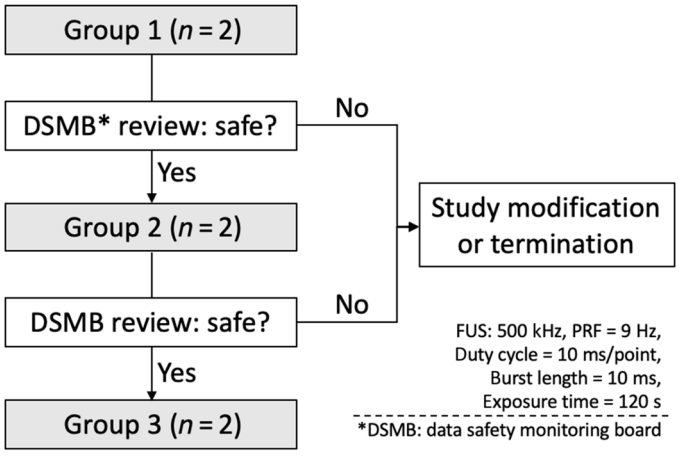

Fig. 8. Diagrammatic protocol of the first-in-human phase 1/2a dose escalation trial using neuronavigation-guided FUS system. A total of six patients with rGBM were treated with a three-tier escalation of FUS dosage, 0.48, 0.58, and 0.68 MI, respectively, in each group ($n = 2$). A DSMB objectively evaluated the AEs of treated patients before entering to the next level of FUS energy. The parameters of NaviFUS system are shown.

challenges due to human skull bone variance. Chang *et al.* (*50*) have shown that the skull volume of sonication field and the skull density ratio are related to failure of temperature elevation in targeted areas. In our patient selection process, we encountered and excluded two candidates (one with very high skull density and the other with osteoporosis), who would have failed to transmit the desired FUS energy dose. Although extensive studies have investigated how to overcome the skull bone barrier effects (*51*–*53*), variable interindividual differences of physical skull properties may still pose considerable challenges for designing FUS treatment plans for optimal efficacy.

There are several limitations of our study. First, for the three-by-three grid exposure, we observed that the BBB opening in each grid was not consistent, which may be due to tissue vascular structural inhomogeneity. At the current stage, there is no tool that has been developed to allow precise three-dimensional (3D) anatomy registration and alignment among the multiple sequential MR scanning. Data analysis is therefore limited to the total steering treatment volume with the FUS center position having been designated. Future improvement should include the serial image registration to provide precise analysis for every individual focus. Second, the concern of variable penetration in human skulls may also prevent the targeted region from receiving the planned dosing energy. This limitation requires further study, especially with regard to translating experimental immune responses in animal models to clinical scenarios in humans. Third, a range not exceeding a ceiling energy level rather than designating a precise energy value was reported, because the uncertainty exists between the estimated and the actual deposited level of the transcranial FUS exposure level at the target. Although we monitored the backscattered acoustic emission, the signal change was not used to close-loop adapt the exposure level. A second-generation device will incorporate passive cavitation detection for future clinical study. Last, the immunogenic effect induced by FUS-BBB opening is an extrapolation from animal study, although a thorough discussion has been made previously; further clinical study is needed to verify this hypothesis and to test its efficacy on tumor control.

FUS exposure level exceeding 0.8 MI has the potential to induce TIL-related immunogenic response, but side effects may include asymptomatic RBC extravasation, which might be a trade-off, at least based on animal model testing. This double-edged sword, however, might be a general and intrinsic constraint when FUS is used to open the BBB to induce immunosuppressive TME effect. The benefit of incorporating FUS for GBM patient treatment shall further optimized through the comprehensive understanding of the underlying mechanism of this treatment strategy.

MATERIALS AND METHODS

Clinical trial design

Study design and participants

This was a first-in-human, prospective, open-label, single-center, single-arm, dose escalation phase 1 pilot study. The objectives of this study were to investigate safety, feasibility, and the tolerated dose for transiently opening the BBB using the NaviFUS system in patients with rGBM. We hypothesize that patients who receive ultrasonic energy delivered by NaviFUS system concomitant with systemic MB administration will show detectable transient BBB opening via DCE-MRI. This study was conducted in accordance with the Declaration of Helsinki, good clinical practice (GCP) guidelines, and all applicable laws and regulations of the Taiwan Food and Drug Administration. This proposed study was approved by Chang Gung Medical Foundation Institutional Review Board and registered on ClinicalTrials.gov (NCT03626896). All participants provided written informed consent before enrollment after a detailed discussion of the study rationale, risks, and process of the procedure.

Participants

Six > 20-year-old adult patients with rGBM (World Health Organization grade IV) who were scheduled to undergo a surgical resection were enrolled in this study. rGBM was defined as a new contrast enhancing tumor, increased SIC of nonenhancing lesion on T2/FLAIR MRI, and clinical deterioration on regular follow-up (*54*). The planned target region of interest (ROI) for FUS exposure was located at the subcortical region, at least 20 mm under the inner skull surface. The ROI cannot be in the brainstem region or regions associated with critical motor or speech functions. The Karnofsky performance status (KPS) should be >60 for all participants (*55*).

Exclusion criteria included patients with a history of untreated arteriovenous malformation or cerebral aneurysm, acute hemorrhage, cyst within the ROI, patients with severe hypertension at screening (systolic blood pressure of >180 mmHg or diastolic blood pressure of >100 mmHg), and receiving anticoagulant or antiplatelet therapy within 1 week before study treatment. Detailed inclusion and exclusion criteria are listed in Table 1.

All eligible patients were assigned in an open-label manner to three groups ($n = 6$; two patients per group) and received different energy doses (in MI) generated from the NaviFUS system. The energy dose was selected on the basis of the results of preclinical good laboratory practice (GLP) safety studies and other non-GLP primate studies (*56*).

NaviFUS procedure and energy setting

A novel FUS device, NaviFUS system (NaviFUS Inc.), with a frequency of 500 kHz was used. The device is composed of an exposure head fixed on a semirigid mechanical arm linked to a cabinet and a console to integrate the energy source and software computing system (Fig. 7). The NaviFUS system is designed to be compatible with

the Medtronic StealthStation S7 neuronavigation system with a fixed supplementary phantom probe on the exposure head providing its reference coordinate. The whole system is mobile.

Before the actual FUS treatment procedure, a neurosurgeon-designed treatment plan of the trajectory to the targeted ROI is documented for review and approved by study principal investigators. To minimize risk, ROIs were selected to avoid the major vasculature and their branches. On the day of the procedure, the patient was put on a treatment table with proper semirigid support of the patient's head and neck. After successful neuronavigation system registration, a real-time simulation of FUS energy trajectory was monitored by the physician. After confirming the target and trajectory, the location of the FUS exposure probe was locked by the neurosurgeon. Patients were then intravenously administered a weight-based MB contrast (SonoVue, 0.1 ml/kg; maximal, 4.8 ml). The patient was awake throughout the whole procedure, and any patient feedback was immediately available. After completing the sonication procedure, a DCE-MRI was immediately performed to verify BBB opening. Patients were then admitted to the neurosurgical ward for postprocedure observation and preparation for definitive surgical resection.

For energy dose selection, the initial FUS dose does not exceed 0.48 MI at target, because this corresponds to the threshold for BBB opening in previous preclinical studies (*57*, *58*). The highest 0.68-MI dose is supported by prior GLP safety tests in rats and beagle dogs. Two other non-GLP preclinical toxicology reference studies also support that the maximum of 0.68 MI at target is safe (*56*, *59*). Furthermore, the SonoCloud clinical study (NCT02253212) reported the application of five different ultrasound doses on human brains. No ultrasound-related DLT was found in the range of 0.5 to 1.1 MI. Therefore, in this study, energy doses of 0.48, 0.58, and 0.68 MI were applied. After completing treatment in each group ($n = 2$), a data and safety monitoring board (DSMB) reviewed any AE reports to decide whether the study can proceed to the next energy level (Fig. 8). Additional sonication parameters used in patient treatment are listed as follows: total exposure time, 120 s; focal scanned matrix, 3 × 3 (gap between adjacent focus, 5 mm); pulse repetition frequency, 9 Hz; burst length/focus exposure, 10 ms. A three-by-three grid of FUS spots was steered at the selected target brain tissue (estimated −3-dB covering volume per spot of 0.18 cm^3), with the cross-sectional distance of adjacent focus was set to 5 mm. The pulse repetition frequency of FUS exposure was set to 9 Hz to allow the completion of nine-spot steering switch for every second during the exposure duration (i.e., 120 s).

CT and MRI acquisition

To obtain bone porosity information for personalized treatment planning, head CT scans of every enrolled patient were obtained before treatment. In addition, 1.5-T MRI (MAGNETOM Espree, Siemens, Germany) was used to acquire MRI images. The target of FUS treatment was selected by neurosurgeons based on the principle of selecting peritumoral nonenhancing regions identified by precontrast and postcontrast T1-weighted image (CE-T1, se2d1; repetition time (TR)/echo time (TE), 454/8.6 ms; field of view (FOV), 230 mm by 200 mm; in-plane resolution, 0.45 mm by 0.45 mm; slice thickness, 4 mm) and T2-weighted positive region (spc3d1; TR/TE, 3200/379 ms; FOV, 256 mm by 256 mm; in-plane resolution, 1 mm by 1 mm; slice thickness, 1 mm). Preoperative T1-weighted CE-MRI was used for neuronavigation registration of intraoperative FUS treatment guidance. After the FUS procedure, every patient underwent DCE-MRI (fl3d1; TR/TE, 4.88/1.68 ms; FOV, 180 mm by 180 mm; in-plane resolution, 1.4 mm by 1.4 mm; slice thickness, 4 mm; flip angles, 5°/10°/15°/20°/25°/30°) with contrast administration [gadolinium–diethylenetriamine pentaacetic acid (Gd-DTPA), Magnevist, Berlex Laboratories, Wayne, NJ, USA; 0.2 ml/kg; infusion rate, 4 ml/s] to determine the extent and magnitude of BBB opening (day 0/dose). Susceptibility-weighted imaging (SWI) MR sequences were also acquired to identify possible hemorrhages using the following parameters: SWI-3D: TR/TE, 49/40 ms; flip angle, 15°; FOV, 230 mm by 230 mm; in-plane resolution, 0.89 mm by 0.89 mm; slice thickness, 2 mm. Twenty-four hours later, the CE-MRI and DCE-MRI examinations were performed again to evaluate BBB closure and DLT (day 1/after dose). If the FUS procedure induced successful BBB opening, then the area treated would show increased SI after contrast injection. However, when the BBB gradually closed after the end of procedure, the SI of enhancement would decrease.

SIC and kinetic analysis

The contrast enhancement among the sonicating regions (ROI comprises of a 3 × 3 sonicating targets; target grid spacing, 5 mm) in CE-T1 image was assessed. The CE-T1 SI change (in percentage) was calculated as $(T1_{post} - T1_{pre})/T1_{pre} \times 100\%$. Here, $T1_{pre}$ indicates SI without contrast agent administration, whereas $T1_{post}$ indicates SI with Gd-DTPA administration. The CE-T1 change was analyzed at day 0 [visit 2 (dose)] and day 1 [visit 2 (postdose)], and the change between two visits (day 0 versus day 1), defined as visit 2 (dose) − visit 2 (postdose), was used to evaluate the BBB closure (concept shown in fig. S5).

In addition, all DCE-MRI series were used to characterize the kinetic behavior of the FUS target. To calculate the kinetic parameters K_{trans} [the transfer rate constant from the intravascular system to the extracellular extravascular space (EES)] and V_e (distribution volume of the contrast agent in the EES), contrast concentrations were calculated from SI changes of the DCE-MRI first, and then, the contrast concentration curve was fit to the extended Kety model (*60*–*62*). The detailed analysis methods were similar to those in Chai *et al.* (*63*). All kinetic parameters were fitted pixel by pixel, using the least squares function in the MATLAB optimization toolbox (MathWorks Inc., Natick, MA, USA) to generate kinetic parameter maps.

The participant was included on the basis of their diagnostic MRI (typically only CE-T1 was presented). Once the patient has been recruited, the participant conducted DCE-MRI at day 0 (immediately after FUS) and day 1 (24 hours after FUS). Because of the consideration of administering multiple Gd-DTPA MR contrast agent in patients with rGBM, we had difficulty to obtain DCE-MRI for the baseline of K_{trans} and V_e in the patient screening phase. As an alternative, we analyzed the screening CE-T1 image and identified the same non-FUS spot both at the target and tumor peripheral location (positions identical to days 0 and 1) to confirm the baseline SIC. The serial CE-T1 SIC at three different time points (before FUS, 0.5 hours; after FUS, 24 hours) was analyzed in both control and FUS areas (see fig. S2).

Outcome evaluation

The primary end point was evaluating the safety of transient BBB opening by the FUS system in patients with rGBM. Successful BBB opening and restoration were determined by gadolinium leakage immediately after sonication and by reduced or absence of enhancement 24 hours after sonication at the target region on T1-weighted CE-MRI.

The safety end point parameters included the following: (i) DLT, defined as the occurrence of a grade 3 or greater AE related to the FUS exposure from day 0 (day of procedure) to day 7 ± 3, which included a corresponding neurological deficit in the region of the FUS treatment; localized brain edema (not preexisting before the FUS treatment); progression of cerebral midline shifts or brain herniation requiring salvage surgery; irreversible focal encephalopathy; or significant bleeding or ischemia in the area of the BBB opening (more than 1 cm in diameter observed for T2* or SWI, occurring within 2 days of the FUS treatment); and (ii) AEs, defined according to the Common Terminology Criteria for Adverse Events guideline, and an SAE, considered if a grade 3 or higher AE occurred. Clinical parameters including vital signs, physical examination, neurological examination, KPS, mini-mental state examination, and laboratory tests were performed until after FUS 1 month for each patient.

Secondary outcomes were to evaluate tolerated dosage using the FUS system for transient BBB disruption. If patients could not tolerate or show DLTs for a particular FUS level, then the dosage from the previous tolerated lower FUS dose group was considered as the maximum tolerated dose.

Histological examination

FUS-targeted peritumoral or tumoral tissues were collected during tumor resection 7 days after sonication. Paraformaldehyde-fixed and paraffin-embedded methods were used to prepare 4-μm-thick sections for IHC analysis. Anti-CD4 antibody (Novocastra, NCL-L-CD4-368) was used to identify helper T lymphocytes ($CD3^+/CD4^+$ HTL); anti-CD8 antibody (Abcam, ab17147) was used to specifically bind to cytotoxic T lymphocytes ($CD3^+/CD8^+$ CTL). FOXP3 marker (eBiocsience, 14-4777) was used for regulatory T cells (T_{regs}). Anti-CD68 antibody (Abcam, ab955) was applied for macrophages.

Preclinical study design

Rat glioma model

All animal experiments were approved by Institutional Animal Care and Use Committee (Chang Gung University, Taoyuan, Taiwan) and adhered to the experimental animal care guidelines. The pathogen-free male Fischer 344 rats, aged 5 to 6 weeks, were purchased from the National Laboratory Animal Center (Taipei, Taiwan). C6 glioma cells were harvested by means of trypsinization and cultured at a concentration of 5×10^4 cells per microliter for implantation. A total of 4 μl of C6 glioma cell suspension was implanted at a depth of 5 mm from the brain surface. Tumor cell injection was performed over a 5-min period, and the needle was withdrawn over another 2 min. Control rats were injected with C6 glioma cells but received sham ultrasound procedure with no energy. Tumors were allowed to grow for 14 days. A total of 20 rats were equally divided into six groups: control/day 0 ($n = 3$), control/day 7 ($n = 3$), 0.63 MI/day 0 ($n = 4$), 0.63 MI/day 7 ($n = 4$), 0.81 MI/day 0 ($n = 3$), and 0.81 MI/day 7 ($n = 3$). Immediately after MB-FUS and sham procedures, a DCE-MRI was performed to compare and quantify BBB permeability. Last, animals were euthanized 5 hours (day 0) and 7 days (day 7) after FUS treatment for histological examinations, respectively.

FUS equipment and sonication

Animals were shaved to expose scalps for FUS treatment and anesthetized with isoflurane (1 to 2%). A catheter (PE-50, Alzet, Cupertino, CA) was inserted in the tail vein for intravenous MB delivery. Each rat was placed directly under the 4 cm by 4 cm window of an acrylic tank, which was filled with deionized, degassed water and sealed with a thin film to allow penetration of ultrasound energy. Ultrasonic gel was used to fill the spaces between the animal's head and the thin-film window. A preclinical-purposed FUS transducer (IMASONIC, Besancon, France; diameter, 60 mm; radius of curvature, 80 mm; frequency, 400 to 600 kHz) was used, mounted, and positioned on the water tank to generate concentrated ultrasound energy to mimic clinical FUS exposure. An arbitrary function generator (33120A, Agilent, Palo Alto, CA; DS345, Stanford Research Systems, Sunnyvale, CA) was used to generate the driving signal fed to a radiofrequency power amplifier (150A100B, Amplifier Research, Souderton, PA, USA) operating in burst mode. After MB injection, burst-tone mode ultrasound was delivered at a pressure of 0.63 or 0.81 MPa (measured in free field via a calibrated polyvinylidene difluoride hydrophone (Onda, Sunnyvale, CA, USA) to the left hemisphere of each rat with the center of the focal zone positioned at the implanted tumor region (burst length, 10 ms; pulse repetition frequency, 1 Hz; total sonication duration, 120 s). The target was located 1 mm behind the bregma, 3 mm left of the midline, and at a 5-mm depth from scalp.

MRI and analysis

All MRI were acquired on a 7-T MR scanner (ClinScan, Bruker, Germany; 7 T) using a four-channel surface coil. Animals were placed in an acrylic holder and anesthetized with isoflurane gas (1 to 2%) at 50 to 70 breaths/min during the entire MRI procedure. All animals were immediately relocated into the MR scanning room after sonication and sham procedures. DCE-MRI imaging was performed to evaluate the kinetic change of the BBB opening. The imaging parameters were as follows: fl3d1: TR/TE, 2.3/0.76 ms; slice thickness, 0.8 mm; flip angles, 5°/10°/15°/20°/25°/30°; matrix size, 192 by 132. Total 128 image datasets were acquired for 5 min. After completing the 10th acquisition, an intravenous bolus of gadolinium (dose, 0.3 ml/kg; Gd-DTPA, Magnevist, Berlex Laboratories, Wayne, NJ, USA) was administered for dynamic acquisition. The infusion rate was 6 ml/min, and Gd-DTPA was mixed with 0.2 ml of saline and heparin. After DCE-MRI acquisition, contrast-enhancing T1-weighted images were acquired to confirm BBB opening region. The following parameters were used: fl2d1: TR/TE, 322/3.8 ms; FOV, 34 mm by 40 mm; in-plane resolution, 0.156 mm by 0.156 mm; slice thickness, 0.8 mm. SWI sequences were also acquired for identifying possible tissue hemorrhage using the following parameters: swi3d1; TR/TE, 30/18 ms; flip angle, 40°; FOV, 32 mm by 40 mm; in-plane resolution, 0.08 mm by 0.08 mm; slice thickness, 0.6 mm.

All DCE-MRI series were also used to characterize the kinetic behavior of the FUS sonication region and generated K_{trans}/V_e maps (calculated method was described in previous section). Three circular ROIs were assigned at the tumor region, tumor periphery, and contralateral control region to calculate average kinetic values for the FUS-induced BBB opening analysis.

Histological examination

To confirm the FUS-induced local immune response, animals were euthanized 5 hours and 7 days after MB-FUS treatment. Paraformaldehyde-fixed and paraffin-embedded methods were used to prepare 10-μm-thick sections for IHC analysis. Anti-CD4 antibody (Abcam, ab237722) identified helper T lymphocytes ($CD3^+/CD4^+$ HTL) and anti-CD8 antibody (Abcam, ab33786) specifically identified cytotoxic T lymphocytes ($CD3^+/CD8^+$ CTL). FOXP3 marker (Abcam, ab215206) labeled T_{regs}. Anti-CD68 antibody (Abcam, ab125212) labeled macrophages.

All stained tissues were imaged using a Leica Aperio Digital Pathology Slide Scanners CS2. $CD4^+$, $CD8^+$, $CD68^+$, and $FoxP3^+$ cells

were quantified in five fields randomly chosen from each tumor section under a ×20 magnification by Aperio ImageScope (version 12.3, Leica). The immunoreactivity of CD68 was assessed with the ratio of positive stained pixel in tumor area of each section, which was analyzed by QuPath (v.0.12, Queen's University Belfast, Northern Ireland) software. Data were collected from three to four rats per treatment condition, and three to five random regions of interest were imaged and analyzed, representing a tumor section. The value of each tumor section was then normalized with the mean value of animals treated with the same condition and euthanized at 5 hours after MB-FUS treatment. For example, the counts of $CD4^+$ cell of animals that received FUS with 0.63MI, which were euthanized on days 0 and 7 were normalized by the mean counts of $CD4^+$ cell of animals that received FUS with 0.63MI, which were euthanized on day 0. An unpaired t test was conducted between the immune cell counts of animal euthanized on days 0 and 7. When $P < 0.05$, it was considered as significant difference.

SUPPLEMENTARY MATERIALS

Supplementary material for this article is available at http://advances.sciencemag.org/cgi/content/full/7/6/eabd0772/DC1

View/request a protocol for this paper from *Bio-protocol*.

REFERENCES AND NOTES

1. Q. T. Ostrom, H. Gittleman, G. Truitt, A. Boscia, C. Kruchko, J. S. Barnholtz-Sloan, CBTRUS statistical report: Primary brain and other central nervous system tumors diagnosed in the United States in 2011-2015. *Neuro Oncol.* **20**, iv1–iv86 (2018).
2. A. M. Molinaro, J. W. Taylor, J. K. Wiencke, M. R. Wrensch, Genetic and molecular epidemiology of adult diffuse glioma. *Nat. Rev. Neurol.* **15**, 405–417 (2019).
3. G. Reifenberger, H. G. Wirsching, C. B. Knobbe-Thomsen, M. Weller, Advances in the molecular genetics of gliomas—Implications for classification and therapy. *Nat. Rev. Clin. Oncol.* **14**, 434–452 (2017).
4. M. Weller, W. Wick, K. Aldape, M. Brada, M. Berger, S. M. Pfister, R. Nishikawa, M. Rosenthal, P. Y. Wen, R. Stupp, G. Reifenberger, Glioma. *Nat. Rev. Dis. Primers.* **1**, 15017 (2015).
5. R. Stupp, M. E. Hegi, W. P. Mason, M. J. van den Bent, M. J. Taphoorn, R. C. Janzer, S. K. Ludwin, A. Allgeier, B. Fisher, K. Belanger, P. Hau, A. A. Brandes, J. Gijtenbeek, C. Marosi, C. J. Vecht, K. Mokhtari, P. Wesseling, S. Villa, E. Eisenhauer, T. Gorlia, M. Weller, D. Lacombe, J. G. Cairncross, R. O. Mirimanoff; European Organisation for Research and Treatment of Cancer Brain Tumour and Radiation Oncology Groups; National Cancer Institute of Canada Clinical Trials Group, Effects of radiotherapy with concomitant and adjuvant temozolomide versus radiotherapy alone on survival in glioblastoma in a randomised phase III study: 5-year analysis of the EORTC-NCIC trial. *Lancet Oncol.* **10**, 459–466 (2009).
6. R. Stupp, W. P. Mason, M. J. van den Bent, M. Weller, B. Fisher, M. J. Taphoorn, K. Belanger, A. A. Brandes, C. Marosi, U. Bogdahn, J. Curschmann, R. C. Janzer, S. K. Ludwin, T. Gorlia, A. Allgeier, D. Lacombe, J. G. Cairncross, E. Eisenhauer, R. O. Mirimanoff; European Organisation for Research and Treatment of Cancer Brain Tumor and Radiotherapy Groups; National Cancer Institute of Canada Clinical Trials Group, Radiotherapy plus concomitant and adjuvant temozolomide for glioblastoma. *N. Engl. J. Med.* **352**, 987–996 (2005).
7. K. Seystahl, W. Wick, M. Weller, Therapeutic options in recurrent glioblastoma—An update. *Crit. Rev. Oncol. Hematol.* **99**, 389–408 (2016).
8. B. Campos, L. R. Olsen, T. Urup, H. S. Poulsen, A comprehensive profile of recurrent glioblastoma. *Oncogene* **35**, 5819–5825 (2016).
9. National Comprehensive Cancer Network. Bone Cancer (Version 3.2020). https://www.nccn.org/professionals/physician_gls/pdf/cns.pdf. Accessed October 25, 2019.
10. R. Stupp, E. T. Wong, A. A. Kanner, D. Steinberg, H. Engelhard, V. Heidecke, E. D. Kirson, S. Taillibert, F. Liebermann, V. Dbaly, Z. Ram, J. L. Villano, N. Rainov, U. Weinberg, D. Schiff, L. Kunschner, J. Raizer, J. Honnorat, A. Sloan, M. Malkin, J. C. Landolfi, F. Payer, M. Mehdorn, R. J. Weil, S. C. Pannullo, M. Westphal, M. Smrcka, L. Chin, H. Kostron, S. Hofer, J. Bruce, R. Cosgrove, N. Paleologous, Y. Palti, P. H. Gutin, NovoTTF-100A versus physician's choice chemotherapy in recurrent glioblastoma: A randomised phase III trial of a novel treatment modality. *Eur. J. Cancer* **48**, 2192–2202 (2012).
11. R. Stupp, S. Taillibert, A. Kanner, W. Read, D. Steinberg, B. Lhermitte, S. Toms, A. Idbaih, M. S. Ahluwalia, K. Fink, F. Di Meco, F. Lieberman, J. J. Zhu, G. Stragliotto, D. Tran, S. Brem, A. Hottinger, E. D. Kirson, G. Lavy-Shahaf, U. Weinberg, C. Y. Kim, S. H. Paek, G. Nicholas, J. Bruna, H. Hirte, M. Weller, Y. Palti, M. E. Hegi, Z. Ram, Effect of Tumor-treating fields plus maintenance temozolomide vs maintenance temozolomide alone on survival in patients with glioblastoma: A randomized clinical trial. *JAMA* **318**, 2306–2316 (2017).
12. N. J. Abbott, Blood-brain barrier structure and function and the challenges for CNS drug delivery. *J. Inherit. Metab. Dis.* **36**, 437–449 (2013).
13. C. Iadecola, The neurovascular unit coming of age: A journey through neurovascular coupling in health and disease. *Neuron* **96**, 17–42 (2017).
14. C. D. Arvanitis, G. B. Ferraro, R. K. Jain, The blood-brain barrier and blood-tumour barrier in brain tumours and metastases. *Nat. Rev. Cancer* **20**, 26–41 (2019).
15. W. M. Pardridge, The blood-brain barrier: Bottleneck in brain drug development. *NeuroRx* **2**, 3–14 (2005).
16. W. M. Pardridge, Drug and gene delivery to the brain: The vascular route. *Neuron* **36**, 555–558 (2002).
17. N. A. Charles, E. C. Holland, R. Gilbertson, R. Glass, H. Kettenmann, The brain tumor microenvironment. *Glia* **59**, 1169–1180 (2011).
18. D. Hambardzumyan, G. Bergers, Glioblastoma: Defining tumor niches. *Trends Cancer* **1**, 252–265 (2015).
19. K.-T. Chen, K.-C. Wei, H.-L. Liu, Theranostic strategy of focused ultrasound induced blood-brain barrier opening for CNS disease treatment. *Front. Pharmacol.* **10**, 86 (2019).
20. M. K. Gumerlock, B. D. Belshe, R. Madsen, C. Watts, Osmotic blood-brain barrier disruption and chemotherapy in the treatment of high grade malignant glioma: Patient series and literature review. *J. Neurooncol* **12**, 33–46 (1992).
21. A. Rodriguez, S. B. Tatter, W. Debinski, Neurosurgical techniques for disruption of the blood-brain barrier for glioblastoma treatment. *Pharmaceutics* **7**, 175–187 (2015).
22. J. T. Duskey, D. Belletti, F. Pederzoli, M. A. Vandelli, F. Forni, B. Ruozi, G. Tosi, Current strategies for the delivery of therapeutic proteins and enzymes to treat brain disorders. *Int. Rev. Neurobiol.* **137**, 1–28 (2017).
23. M. Westphal, D. C. Hilt, E. Bortey, P. Delavault, R. Olivares, P. C. Warnke, I. R. Whittle, J. Jaaskelainen, Z. Ram, A phase 3 trial of local chemotherapy with biodegradable carmustine (BCNU) wafers (Gliadel wafers) in patients with primary malignant glioma. *Neuro Oncol.* **5**, 79–88 (2003).
24. S. D. Ferguson, K. Foster, B. Yamini, Convection-enhanced delivery for treatment of brain tumors. *Expert Rev. Anticancer Ther.* **7**, S79–S85 (2007).
25. K. Hynynen, N. McDannold, N. Vykhodtseva, F. A. Jolesz, Noninvasive MR imaging-guided focal opening of the blood-brain barrier in rabbits. *Radiology* **220**, 640–646 (2001).
26. K. Hynynen, N. McDannold, N. Vykhodtseva, F. A. Jolesz, Non-invasive opening of BBB by focused ultrasound. *Acta Neurochir. Suppl.* **86**, 555–558 (2003).
27. K. Hynynen, N. McDannold, N. A. Sheikov, F. A. Jolesz, N. Vykhodtseva, Local and reversible blood-brain barrier disruption by noninvasive focused ultrasound at frequencies suitable for trans-skull sonications. *Neuroimage* **24**, 12–20 (2005).
28. N. McDannold, N. Vykhodtseva, K. Hynynen, Targeted disruption of the blood-brain barrier with focused ultrasound: Association with cavitation activity. *Phys. Med. Biol.* **51**, 793–807 (2006).
29. M. Kinoshita, N. McDannold, F. A. Jolesz, K. Hynynen, Noninvasive localized delivery of Herceptin to the mouse brain by MRI-guided focused ultrasound-induced blood-brain barrier disruption. *Proc. Natl. Acad. Sci. U.S.A.* **103**, 11719–11723 (2006).
30. L. H. Treat, N. McDannold, Y. Zhang, N. Vykhodtseva, K. Hynynen, Improved anti-tumor effect of liposomal doxorubicin after targeted blood-brain barrier disruption by MRI-guided focused ultrasound in rat glioma. *Ultrasound Med. Biol.* **38**, 1716–1725 (2012).
31. K.-C. Wei, P.-C. Chu, H.-Y. J. Wang, C.-Y. Huang, P.-Y. Chen, H.-C. Tsai, Y.-J. Lu, P.-Y. Lee, I.-C. Tseng, L.-Y. Feng, P.-W. Hsu, T.-C. Yen, H.-L. Liu, Focused ultrasound-induced blood–brain barrier opening to enhance temozolomide delivery for glioblastoma treatment: A preclinical study. *PLOS ONE* **8**, e58995 (2013).
32. H.-L. Liu, C.-Y. Huang, J.-Y. Chen, H.-Y. Wang, P.-Y. Chen, K.-C. Wei, Pharmacodynamic and therapeutic investigation of focused ultrasound-induced blood-brain barrier opening for enhanced temozolomide delivery in glioma treatment. *PLOS ONE* **9**, e114311 (2014).
33. H. L. Liu, M. Y. Hua, H. W. Yang, C. Y. Huang, P. C. Chu, J. S. Wu, I. C. Tseng, J. J. Wang, T. C. Yen, P. Y. Chen, K. C. Wei, Magnetic resonance monitoring of focused ultrasound/magnetic nanoparticle targeting delivery of therapeutic agents to the brain. *Proc. Natl. Acad. Sci. U.S.A.* **107**, 15205–15210 (2010).
34. C. Y. Ting, C. H. Fan, H. L. Liu, C. Y. Huang, H. Y. Hsieh, T. C. Yen, K. C. Wei, C. K. Yeh, Concurrent blood-brain barrier opening and local drug delivery using drug-carrying microbubbles and focused ultrasound for brain glioma treatment. *Biomaterials* **33**, 704–712 (2012).
35. C. H. Fan, W. H. Lin, C. Y. Ting, W. Y. Chai, T. C. Yen, H. L. Liu, C. K. Yeh, Contrast-enhanced ultrasound imaging for the detection of focused ultrasound-induced blood-brain barrier opening. *Theranostics* **4**, 1014–1025 (2014).
36. D. F. Quail, J. A. Joyce, The microenvironmental landscape of brain tumors. *Cancer Cell* **31**, 326–341 (2017).
37. P. Y. Chen, H. Y. Hsieh, C. Y. Huang, C. Y. Lin, K. C. Wei, H. L. Liu, Focused ultrasound-induced blood-brain barrier opening to enhance interleukin-12 delivery for brain tumor immunotherapy: A preclinical feasibility study. *J. Transl. Med.* **13**, 93 (2015).

38. C. T. Curley, N. D. Sheybani, T. N. Bullock, R. J. Price, Focused ultrasound immunotherapy for central nervous system pathologies: Challenges and opportunities. *Theranostics* **7**, 3608–3623 (2017).
39. O. Cohen-Inbar, Z. Xu, J. P. Sheehan, Focused ultrasound-aided immunomodulation in glioblastoma multiforme: A therapeutic concept. *J Ther Ultrasound* **4**, 2 (2016).
40. P. Y. Chen, K. C. Wei, H. L. Liu, Neural immune modulation and immunotherapy assisted by focused ultrasound induced blood-brain barrier opening. *Hum. Vaccin. Immunother.* **11**, 2682–2687 (2015).
41. K. C. Wei, H. C. Tsai, Y. J. Lu, H. W. Yang, M. Y. Hua, M. F. Wu, P. Y. Chen, C. Y. Huang, T. C. Yen, H. L. Liu, Neuronavigation-guided focused ultrasound-induced blood-brain barrier opening: A preliminary study in swine. *AJNR Am. J. Neuroradiol.* **34**, 115–120 (2013).
42. H. C. Tsai, C. H. Tsai, W. S. Chen, C. Inserra, K. C. Wei, H. L. Liu, Safety evaluation of frequent application of microbubble-enhanced focused ultrasound blood-brain-barrier opening. *Sci. Rep.* **8**, 17720 (2018).
43. S. K. Wu, P. C. Chu, W. Y. Chai, S. T. Kang, C. H. Tsai, C. H. Fan, C. K. Yeh, H. L. Liu, Characterization of different microbubbles in assisting focused ultrasound-induced blood-brain barrier opening. *Sci. Rep.* **7**, 46689 (2017).
44. A. Carpentier, M. Canney, A. Vignot, V. Reina, K. Beccaria, C. Horodyckid, C. Karachi, D. Leclercq, C. Lafon, J. Y. Chapelon, L. Capelle, P. Cornu, M. Sanson, K. Hoang-Xuan, J. Y. Delattre, A. Idbaih, Clinical trial of blood-brain barrier disruption by pulsed ultrasound. *Sci. Transl. Med.* **8**, 343re2 (2016).
45. A. Idbaih, M. Canney, L. Belin, C. Desseaux, A. Vignot, G. Bouchoux, N. Asquier, B. Law-Ye, D. Leclercq, A. Bissery, Y. De Rycke, C. Trosch, L. Capelle, M. Sanson, K. Hoang-Xuan, C. Dehais, C. Houillier, F. Laigle-Donadey, B. Mathon, A. Andre, C. Lafon, J. Y. Chapelon, J. Y. Delattre, A. Carpentier, Safety and feasibility of repeated and transient blood-brain barrier disruption by pulsed ultrasound in patients with recurrent glioblastoma. *Clin. Cancer Res.* **25**, 3793–3801 (2019).
46. T. Mainprize, N. Lipsman, Y. Huang, Y. Meng, A. Bethune, S. Ironside, C. Heyn, R. Alkins, M. Trudeau, A. Sahgal, J. Perry, K. Hynynen, Blood-brain barrier opening in primary brain tumors with non-invasive MR-guided focused ultrasound: A clinical safety and feasibility study. *Sci. Rep.* **9**, 321 (2019).
47. S. H. Park, M. J. Kim, H. H. Jung, W. S. Chang, H. S. Choi, I. Rachmilevitch, E. Zadicario, J. W. Chang, Safety and feasibility of multiple blood-brain barrier disruptions for the treatment of glioblastoma in patients undergoing standard adjuvant chemotherapy. *J. Neurosurg.*, 1–9 (2020).
48. J. Yang, J. Yan, B. Liu, Targeting VEGF/VEGFR to modulate antitumor immunity. *Front. Immunol.* **9**, 978 (2018).
49. H. L. Liu, P. H. Hsu, C. Y. Lin, C. W. Huang, W. Y. Chai, P. C. Chu, C. Y. Huang, P. Y. Chen, L. Y. Yang, J. S. Kuo, K. C. Wei, Focused ultrasound enhances central nervous system delivery of bevacizumab for malignant glioma treatment. *Radiology* **281**, 99–108 (2016).
50. W. S. Chang, H. H. Jung, E. Zadicario, I. Rachmilevitch, T. Tlusty, S. Vitek, J. W. Chang, Factors associated with successful magnetic resonance-guided focused ultrasound treatment: Efficiency of acoustic energy delivery through the skull. *J. Neurosurg.* **124**, 411–416 (2016).
51. G. T. Clement, K. Hynynen, Correlation of ultrasound phase with physical skull properties. *Ultrasound Med. Biol.* **28**, 617–624 (2002).
52. C. W. Connor, K. Hynynen, Patterns of thermal deposition in the skull during transcranial focused ultrasound surgery. *I.E.E.E. Trans. Biomed. Eng.* **51**, 1693–1706 (2004).
53. G. Pinton, J. F. Aubry, E. Bossy, M. Muller, M. Pernot, M. Tanter, Attenuation, scattering, and absorption of ultrasound in the skull bone. *Med. Phys.* **39**, 299–307 (2012).
54. P. Y. Wen, D. R. Macdonald, D. A. Reardon, T. F. Cloughesy, A. G. Sorensen, E. Galanis, J. Degroot, W. Wick, M. R. Gilbert, A. B. Lassman, C. Tsien, T. Mikkelsen, E. T. Wong, M. C. Chamberlain, R. Stupp, K. R. Lamborn, M. A. Vogelbaum, M. J. van den Bent, S. M. Chang, Updated response assessment criteria for high-grade gliomas: Response assessment in neuro-oncology working group. *J. Clin. Oncol.* **28**, 1963–1972 (2010).
55. V. Mor, L. Laliberte, J. N. Morris, M. Wiemann, The Karnofsky performance status scale: An examination of its reliability and validity in a research setting. *Cancer* **53**, 2002–2007 (1984).
56. N. McDannold, C. D. Arvanitis, N. Vykhodtseva, M. S. Livingstone, Temporary disruption of the blood-brain barrier by use of ultrasound and microbubbles: Safety and efficacy evaluation in rhesus macaques. *Cancer Res.* **72**, 3652–3663 (2012).
57. K. Hynynen, N. McDannold, N. Vykhodtseva, S. Raymond, R. Weissleder, F. A. Jolesz, N. Sheikov, Focal disruption of the blood-brain barrier due to 260-kHz ultrasound bursts: A method for molecular imaging and targeted drug delivery. *J. Neurosurg.* **105**, 445–454 (2006).
58. N. McDannold, N. Vykhodtseva, K. Hynynen, Blood-brain barrier disruption induced by focused ultrasound and circulating preformed microbubbles appears to be characterized by the mechanical index. *Ultrasound Med. Biol.* **34**, 834–840 (2008).
59. C. Horodyckid, M. Canney, A. Vignot, R. Boisgard, A. Drier, G. Huberfeld, C. Francois, A. Prigent, M. D. Santin, C. Adam, J. C. Willer, C. Lafon, J. Y. Chapelon, A. Carpentier, Safe long-term repeated disruption of the blood-brain barrier using an implantable ultrasound device: A multiparametric study in a primate model. *J. Neurosurg.* **126**, 1351–1361 (2017).
60. P. S. Tofts, Modeling tracer kinetics in dynamic Gd-DTPA MR imaging. *J. Magn. Reson. Imaging* **7**, 91–101 (1997).
61. P. S. Tofts, G. Brix, D. L. Buckley, J. L. Evelhoch, E. Henderson, M. V. Knopp, H. B. Larsson, T. Y. Lee, N. A. Mayr, G. J. Parker, R. E. Port, J. Taylor, R. M. Weisskoff, Estimating kinetic parameters from dynamic contrast-enhanced T_1-weighted MRI of a diffusable tracer: Standardized quantities and symbols. *J. Magn. Reson. Imaging* **10**, 223–232 (1999).
62. P. S. Tofts, A. G. Kermode, Measurement of the blood-brain barrier permeability and leakage space using dynamic MR imaging. 1. Fundamental concepts. *Magn. Reson. Med.* **17**, 357–367 (1991).
63. W. Y. Chai, P. C. Chu, M. Y. Tsai, Y. C. Lin, J. J. Wang, K. C. Wei, Y. Y. Wai, H. L. Liu, Magnetic-resonance imaging for kinetic analysis of permeability changes during focused ultrasound-induced blood-brain barrier opening and brain drug delivery. *J. Control. Release* **192**, 1–9 (2014).

Acknowledgments: We are grateful to all participants who volunteered to participate in this study. **Funding:** This study is sponsored by the Ministry of Science and Technology, Taiwan (grants 105-2221-E-182-022 and 106-2221-E-182-002), Chang Gung Memorial Hospital, Linkou (grants CIRPD2E0051-53 and CMRPD2D0111-13), and National Health Research Institute grant NHRI-EX109-10502NI. This study is also supported by the Clinical Trial Center, Chang Gung Memorial Hospital, Linkou, Taiwan (funded by the Ministry of Health and Welfare of Taiwan; grants MOHW107-TDU-B-212-123005, MOHW108-TDU-B-212-133005, and MOHW109-TDU-B-212-114005). This study is also sponsored and technically supported by NaviFUS Inc.
Author contributions: H.-L.L. and K.-C.W. developed the hypothesis. K.-T.C., H.-L.L., W.-Y.C., and K.-C.W. designed the paradigm. K.-C.W., K.-T.C., Y.-J.L., P.-Y.C., and H.-C.T. were clinical investigators on the study. C.-Y.H., C.-J.L., and W.-Y.C. performed animal model experiments and data collection. K.-T.C. and H.-L.L. analyzed data with support from W.-Y.C. and C.-J.L. H.-L.L., K.-C.W., and J.S.K. supported the study team with regulatory issues, logistics, and clinical support. K.-T.C., W.-Y.C., and H.-L.L. wrote the manuscript, with substantial support from all authors. **Competing interests:** H.-C.T., H.-L.L., and K.-C.W. are inventors on a patent entitled "Neuronavigation-guided focused ultrasound system and method thereof," which was granted in multiple nations, including United States (no. 10166410, 1 January 2019), Canada (no. CN103479403B, 21 August 2018), European Union (no. EP2858619A4, 18 May 2017), Australia (no. 2013271506, 28 June 2016), Japan (no. 6188036, 10 August 2017), Korea (no. 101851243, 11 July 2018), and China (no. CN103479403B, 22 June 2016). This is the only patent related to this study. Patent application was sent in 2015 and issued by the Chang Gung University. H.-L.L. provides technical consulting service for NaviFUS Inc. The other authors declare that they have no competing interests. **Data and materials availability:** All data needed to evaluate the conclusions in the paper are present in the paper and/or the Supplementary Materials. Additional data related to this paper may be requested from the authors.

Submitted 30 May 2020
Accepted 18 December 2020
Published 5 February 2021
10.1126/sciadv.abd0772

Citation: K.-T. Chen, W.-Y. Chai, Y.-J. Lin, C.-J. Lin, P.-Y. Chen, H.-C. Tsai, C.-Y. Huang, J. S. Kuo, H.-L. Liu, K.-C. Wei, Neuronavigation-guided focused ultrasound for transcranial blood-brain barrier opening and immunostimulation in brain tumors. *Sci. Adv.* **7**, eabd0772 (2021).